Native defects and complexes in SiC

2001 J. Phys.: Condens. Matter 13 9027

(http://iopscience.iop.org/0953-8984/13/40/319)

INSTITUTE OF PHYSICS PUBLISHING JOURNAL OF PHYSICS: CONDENSED MATTER

J. Phys.: Condens. Matter **13** (2001) 9027–9037 PII: S0953-8984(01)24507-X

Native defects and complexes in SiC

F Bechstedt, A Fissel, J Furthmüller, U Grossner and A Zywietz

Institut für Festkörpertheorie und Theoretische Optik, Friedrich-Schiller-Universität, 07743 Jena, Germany

Received 2 May 2001
Published 20 September 2001
Online at stacks.iop.org/JPhysCM/13/9027

Abstract

Prototypical native defects, in particular monovacancies, are studied using *ab initio* density functional theory and the local spin-density approximation. Several properties such as the energetics, geometry, electronic structure, and spin states are discussed regarding their dependence on the chemical nature, the preparation conditions, and the polytype of the SiC crystal. Consequences of the defects are derived for the doping behaviour, electrical properties, and photoluminescence spectra.

1. Introduction

The physical properties of silicon carbide (SiC) make this wide-band-gap semiconductor well suited for high-temperature, high-power, and high-frequency applications. A striking property of SiC is its polytypism. The compound exists in more than 200 different polytypes of which the 3C, 4H, 6H, and 15R structures are the most common [1]. The accompanying variation of the indirect fundamental gap between 2.39 eV (3C) and 3.26 eV (4H) [2] makes SiC also interesting for application in heterostructure devices, e.g. in twinning superlattices [3].

Defects and their complexes play an important role. To a great extent the electrical and optical properties of SiC are governed by native defects, which also exhibit interesting physics of their own. They are observed in as-grown crystals and layers as well as in irradiated samples. The monovacancies are prototypical examples in this respect. In SiC the situation is markedly different from that encountered in common semiconductors like silicon. Because of the stronger chemical bonding in this hard compound, the mobility of such point defects is reduced. They are thermally stable at room temperature, and far above [4]. In contrast to the case of silicon, antisites also occur in the compound semiconductor SiC. These native point defects can give rise to energy levels in the fundamental gap and, hence, exist in different charge states [5, 6]. Consequently, they may influence the doping efficiency [7].

Strong indications for certain defects or defect complexes come from characteristic sharp lines in photoluminescence (PL) spectra. One prototypical defect responsible for such emission lines in the low-temperature PL spectra is the so-called D_1 centre [8]. Its fingerprint is an efficient luminescence at a photon energy 0.35–0.45 eV below the excitonic gap independent of the polytype. The most important L_1 line is followed by characteristic phonon-assisted

structures [9]. It has been observed for different polytypes after irradiation [9–13], but also for as-grown material after quenching from the growth temperature and epitaxial layers grown by chemical vapour deposition (CVD) or solid-source molecular beam epitaxy (MBE) [14–16]. For 4H-SiC the L_1 line appears at about 2.901 eV [11, 12], whereas 3C-SiC shows this line at about 1.972 eV [17]. Other strong indications for a native defect, perhaps a silicon vacancy [18], are the characteristic PL bands with no-phonon lines at 1.121 eV for 3C-SiC [19], 1.438 and 1.352 eV for 4H-SiC [20, 21], or 1.433, 1.398, and 1.368 eV for 6H-SiC [20, 21]. In contrast to the positions of the L_1 lines, these PL bands depend only weakly on the polytype.

Besides the direct influence on the doping efficiency [7] of e.g. donating electrons [5], native defects may influence the effect of dopants by forming complexes. One example concerns the interpretation of the deep boron acceptor as a boron (B) on a silicon position with an adjacent vacancy [22, 23]. There is also a shallow boron acceptor, the geometry and the sublattice site, B_{Si} or B_C, of which are under discussion [24, 25]. There are indications that the preferential occupation of a Si or C site depends on the preparation conditions, i.e. C-rich or Si-rich conditions [24, 26]. These findings seem to be in agreement with results of C/B coimplantation experiments [27].

In the present paper we discuss the relationship between energetics, geometry, and electronic states for native defects in 3C- and 4H-SiC. Monovacancies are considered as prototypical defects, but antisites are also studied. B atoms adsorbed at a surface are considered as defect complexes. The computational method is described in section 2. The following sections 3 and 4 discuss the formation of native defects and the resulting electronic states. This is completed by studies of boron at surfaces in section 5. Finally, a brief summary is given.

2. Computational method

The calculations are based on density functional theory (DFT) [28] in the local spin-density approximation (LSDA) [29]. Explicitly we use the Vienna *Ab initio* Simulation Package (VASP) [30]. The interaction of the valence electrons with the atomic cores is treated using non-norm-conserving Vanderbilt pseudopotentials [31]. Their supersoftened form is especially important for the treatment of first-row elements such as C and B. It allows the restriction of the plane-wave expansion of the single-particle eigenfunctions to a cut-off energy of 13.4 Ryd. This corresponds to about 55 plane waves per atom. Exchange and correlation are described in the parametrization of Perdew and Zunger [32]. In order to avoid partial errors due to the use of frozen cores, non-linear core corrections are included. For arbitrary spin polarization the correlation energy is interpolated between the non-polarized and fully polarized case as for the exchange energy [33]. The method described gives for the defect-free polytypes 3C and 4H lattice constants slightly smaller than the experimental ones. The cubic lattice constant of the zinc-blende polytype with T_d^2 symmetry amounts to $a_0 = 4.332$ Å, whereas the two hexagonal lattice constants of 4H-SiC (C_{6v}^4) are $a = 3.061$ Å and $c = 10.013$ Å. The internal deformations of the bonding tetrahedra are small (see [34]). Without quasiparticle corrections [35] DFT-LDA gives the values 1.33 eV (3C-SiC) and 2.23 eV (4H-SiC) for the energy gaps which are about 1 eV smaller than the experimental energies [2].

Extremely large supercells with 216 atoms (3C) or 128 atoms (4H) are treated to avoid too strong defect–defect interactions and electrostatic effects. The total-energy minimization with respect to the atomic coordinates is performed by a conjugate-gradient technique [30]. Within the structural optimization a $2 \times 2 \times 2$ special-point mesh [36] is used for the $\boldsymbol{k}$-space

sampling. In order to describe excited defect states we take into account the constraint of a hole in the lowest a_1-derived single-particle defect state. However, the effects of the excitation as well as of the spin polarization are described restricting the sampling to the Γ point. The influence of unphysical $\boldsymbol{k}$-induced splittings and dispersions is suppressed in this way. Details of the computational method can be found in reference [5]. In the case of B adsorption the Si-terminated SiC(111) surfaces are modelled by repeated slabs containing six Si–C bilayers and a vacuum region of the same thickness. The C-terminated bottom layers of the slabs are saturated with atomic hydrogen [37]. In the case of a two-dimensional $\sqrt{3} \times \sqrt{3}$ translational symmetry, supercells with effectively 72 atoms are taken into account.

3. Formation of charged native defects

First, we consider monovacancies V_X^q in the charge states $q = 2+, +, 0, -, 2-$. Independent of the polytype, 3C or 4H, the ground state of a C-site vacancy generally exhibits a remarkable Jahn–Teller distortion apart from the double positively charged one. This can be easily explained for the cubic polytype. However, disregarding the small deformations of the bonding tetrahedra, locally the same happens also in the 4H case. There is a tendency for relaxation towards D_{2d} symmetry as a consequence of a pairing mode. The Si dangling bonds of the C vacancy overlap partially. In addition to an inward (positively charged) or outward (negatively charged) breathing relaxation, the defect systems gain energy by formation of bonded pairs of first-nearest-neighbour atoms. This is demonstrated in figure 1. Lowering the local symmetry from T_d to D_{2d}, the threefold-degenerate t_2 defect level (without spin) splits into a lower b_2 state and a higher twofold-degenerate e state. This mechanism occurs for V_C^+, V_C^0, and V_C^-. Further local symmetry reductions do not occur for V_C^{2-}. In 3C the additional electrons occupy conduction band states. Hence, negatively charged carbon vacancies do not exist in

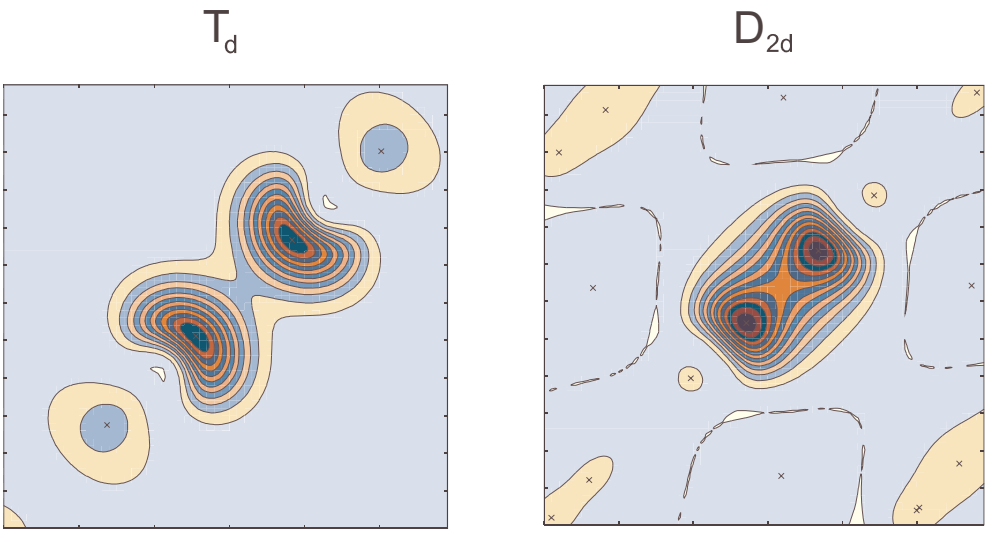

Figure 1. Contour plots of the square of the wave function of the highest occupied defect state of V_C^0 in 3C-SiC in a plane perpendicular to a cubic direction. Two local symmetries T_d and D_{2d} are allowed.

(This figure is in colour only in the electronic version)

3C. However, they occur in the 4H case with a wider energy gap. Additionally, the crystal-field splitting acts in the hexagonal polytype.

V_C^{2+} exhibits a huge inward breathing mode, whereas V_C^0 shows the above-mentioned pronounced pairing mechanism. The large geometrical changes in the V_C^0 and V_C^{2+} cases in comparison to the intermediate charge state $q = +$ result in a negative-U behaviour [38]. We calculate a Hubbard $U = E_{tot}(V_C^{2+}) + E_{tot}(V_C^0) - 2E_{tot}(V_C^+) = -0.35$ eV [39]. Consequently, the single positively charged C vacancy should be unstable in thermodynamic equilibrium. For 4H-SiC we calculate similar values, $U = -0.29$ and -0.24 eV, depending on the cubic (k) or hexagonal (h) lattice site [5]. However, because of the larger energy gap, the double negatively charged vacancy can also occur as a stable defect. As a consequence one observes a negative-U behaviour with $U = -0.29$ eV independent of the lattice site also for the defects with additional electrons.

The situation is quite different for the Si-site vacancies [5, 40]. Because of the strong localization of the C dangling bonds and the SiC lattice constant, only an outward breathing relaxation may occur [41]. The defect system can gain additional energy by a spin splitting of the t_2 levels. In the case of the single positively charged, neutral, and negatively charged Si-site vacancies, high-spin states are predicted independent of the polytype in agreement with Hund's rule. The total spins $S = 0$ (V_{Si}^{2+}), 1/2 (V_{Si}^{+}), 1 (V_{Si}^{0}), 3/2 (V_{Si}^{-}), and 1 (V_{Si}^{2-}) are obtained for the ground states [5, 40]. Meanwhile, there is reason to doubt the DFT-LSDA result of a $^3T_1$ ground state for the neutral Si vacancy, at least in the 3C-SiC case [42]. More careful LSDA studies end up with a mixed-spin state, $^1E + {}^3T_1$ [43]. However, because of principal limitations of the DFT-LSDA a pure-spin multiplet ^1E cannot be derived. Fortunately, despite the spin problem the results for the atomic geometry and the energetics do not change very much. We estimate an energy difference between ^1E and $^3T_1$ of about 0.04 eV, which slightly increases upon inclusion of gradient corrections in the exchange–correlation energy.

In thermal equilibrium the concentrations of the defects are mainly determined by their formation energies. We adapt the formalism of Zhang and Northrup [44]. All chemical potentials and heats of formation are taken from *ab initio* calculations as described in section 2. The Fermi level E_F is allowed to vary in an interval defined by the experimental gap energy E_g [2]. Results for 3C-SiC are presented in figure 2. The results for 4H-SiC are rather similar. There is only a small difference in vacancy formation on cubic and hexagonal sites. In general,

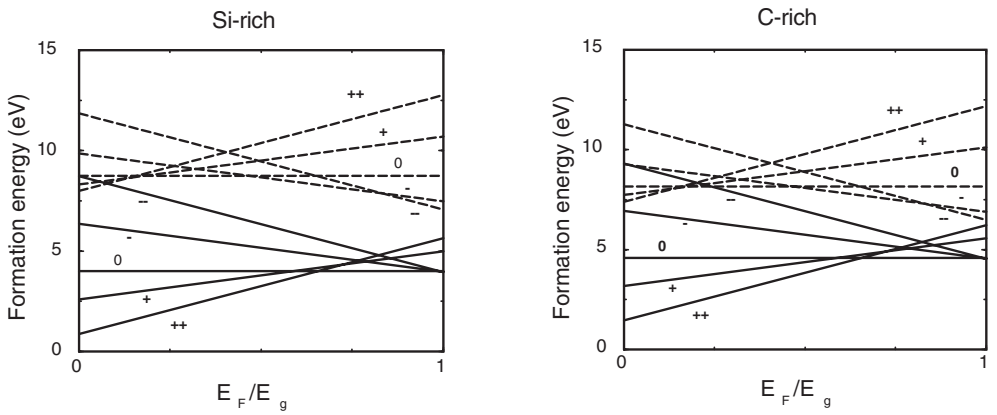

Figure 2. Formation energies of C (solid lines) and Si (dashed lines) vacancies in 3C-SiC versus the Fermi level position in the fundamental energy gap. The most extreme preparation conditions are considered.

the cubic sites are preferred for carbon vacancies. The most important change happens due to the increase of the energy gap by about 1 eV. The slopes in figure 2 indicate that in highly n-doped 4H the negatively charged C vacancies should possess the lowest formation energies. The lowest formation energies (and, hence, highest defect concentrations) are found for V_C^{2+} under p-type doping and both Si-rich and C-rich preparation conditions. That means, under equilibrium conditions, that in the p-type limit the carbon vacancy is a double donor, regardless of stoichiometry [5,7]. These findings may explain why as-grown cubic SiC is always weakly n-type as well as the lowered doping efficiency of acceptors [45–47]. It seems that 40–60% of Al acceptors are compensated in p-type epilayers [47].

The formation energies of carbon antisite defects in 3C-SiC are shown in figure 3. The underlying local symmetry is T_d. Test calculations employing starting configurations with D_{2d} or C_{3v} symmetry showed that the defect system relaxes into a T_d configuration. In contrast to these findings we expected a planar C_{3v} configuration of four carbon atoms with sp^2 hybridization and an empty p dangling-bond orbital. It turns out that the negatively charged carbon antisites C_{Si}^- have the lowest formation energy of all native defects studied in n-type 3C-SiC grown under C-rich conditions, in agreement with other published theoretical studies [6, 7]. However, the carbon antisite is not electrically active. It does not induce any state in the fundamental gap.

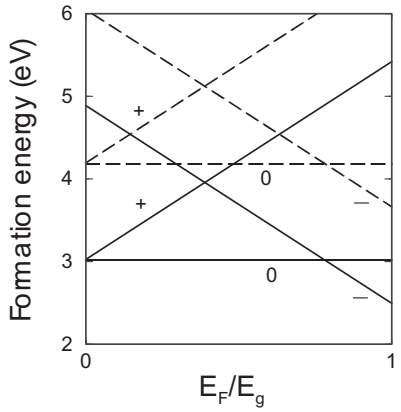

Figure 3. Formation energies of C_{Si}^q antisites in 3C-SiC versus the Fermi level position for two different preparation conditions. Solid lines: C-rich; dashed lines: Si-rich.

4. Ionization levels and intravacancy transitions

The (donor-like) ionization levels ($q - 1/q$) of a defect are independent of the preparation conditions, i.e. the actual values of the chemical potentials of the species involved. They are defined as the positions of the Fermi level E_F at which the charge states of the defects change from $q - 1$ to q. Results are presented in figure 4. They indicate similarities of the level schemes of 3C and 4H with respect to the valence band maximum. The main variation is due to the wider energy gap in 4H. Deep mid-gap defect levels can more or less be used to align the band structures of 3C- and 4H-SiC according to the Langer–Heinrich rule [48].

Figure 5 presents the low-temperature PL spectra of 4H- and 3C-SiC layers grown by means of solid-source MBE [16]. They show the well-known emission lines of the D_1 defect centre, both the zero-phonon L_1 line and the phonon replica. In table 1 we compare

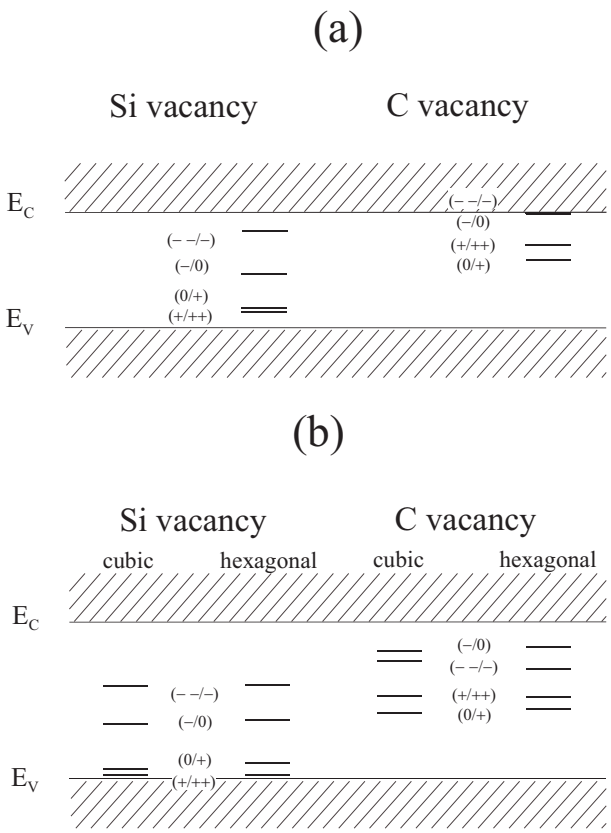

Figure 4. Energy-level schemes for silicon and carbon vacancies in 3C-SiC (a) and 4H-SiC (b).

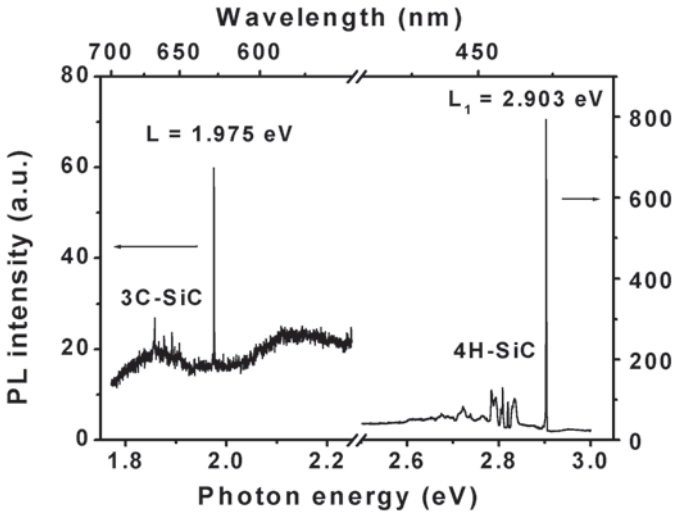

Figure 5. Photoluminescence spectra of 4H- and 3C-SiC layers grown homoepitaxially by means of MBE.

Table 1. Ionization energies (in eV) of Si (C) vacancies in 3C- and 4H-SiC with respect to the conduction band minimum. Cubic (k) and hexagonal (h) sites are indicated. For comparison the L_1 emission line positions are also given.

	k (3C)	h (4H)	k (4H)
(+/2+)	2.05 (0.67)	3.18 (1.58)	3.20 (1.58)
(0/+)	1.96 (0.98)	2.95 (1.82)	3.06 (1.89)
(−/0)	1.28 (—)	1.98 (0.65)	2.07 (0.52)
(2−/−)	0.41 (—)	1.31 (0.84)	1.32 (0.81)
L_1	1.97	2.90	

the line positions with calculated donor ionization energies. The comparison shows that the donor ionization levels (0/+) of silicon vacancies in 3C and 4H (hexagonal site) nearly give the positions of the luminescence lines. Thereby, the binding energy of about 0.03–0.06 eV [11–13] of the bound exciton is neglected and an inaccuracy of about 0.1 eV of the theoretical level positions is taken into account. The advantage of this identification is the explanation of the polytype dependence of the L_1 line and of the non-occurrence of a second line for 4H. The splitting of the two (0/+) energies of cubic and hexagonal sites is rather large, so electron–hole pairs recombine via the lower-energy transition.

These results suggest the conclusion that a Si vacancy, or more strictly speaking a C dangling bond, is involved in the D_1 centre. There are also arguments against this interpretation. The Si vacancy formation energies are generally larger than those of C vacancies (cf. figure 2). However, the MBE growth of SiC [16] happens under conditions where the concentration of Si adatoms is nearly given by its equilibrium value. No accumulation of Si occurs on the growing SiC surface. On the other hand, desorption of carbon or carbon-bearing species, such as Si_2C and SiC_2, can be neglected.

In addition, it has been suggested that Si vacancies are unstable in thermodynamic equilibrium against a transformation into a defect complex according to $V_{Si}^0 \rightarrow V_C^0 + C_{Si}^0$, because of their larger formation energy in comparison to that of C vacancies [49]. However, there exists an energy barrier for this process of about 1.8 eV which is much higher than the thermal energy at the growth temperature of 1500 K (3C) or 1600 K (4H).

The question arises of whether other PL lines, e.g. that at 1.35 and 1.44 eV for 4H [20,21] or 1.12 eV for 3C [19], can be related to native defects such as vacancies or not. To answer this question, we study the lowest intravacancy transition energies of Si vacancies in 3C- and 4H-SiC as total-energy differences $\hbar\omega = E_{tot}(V_{Si}^q, \text{excited}) - E_{tot}(V_{Si}^q, \text{ground})$. Thereby, the excited state is described using the constraint of a hole in the low-energy a_1 defect state. Results are listed in table 2. In the 3C case we also give transition energies that are corrected by about 0.15 or 0.35 eV, in order to account for the strong dispersion of the lowest a_1 defect band [41]. Despite the large supercells of 216 atoms, such a strong dispersion occurs due to the vacancy–vacancy interaction and the mixing with bulk-like contributions.

Interestingly all of the intravacancy transition energies considered in table 2 vary little with the charge state of the vacancy V_{Si}^q and the polytype of the host, in particular considering only cubic lattice sites. The reason is that the charge state q shifts both participating single-particle levels a_1 and t_2 in the same manner. The participating orbitals are combined by the same C hybrids in more or less the same distance. The large difference in the V_{Si}^{2-} case is a consequence of the fact that in 3C the $t_2^{\uparrow}$ level lies above the conduction band minimum. For 4H-SiC the site dependence has to be taken into consideration. The transitions at hexagonal

Table 2. Lowest intradefect transition energies (in eV) for V_{Si}^{q} in 3C- and 4H-SiC. The inequivalent lattice sites, k and h, are distinguished in 4H. In the 3C case the energies corrected by the strong $\boldsymbol{k}$-dispersion of the a_1 defect band are given in parentheses.

Charge state q	Transition	3C (k)	4H (k)	4H (h)
+	$a_1^2 t_2^{\uparrow} \rightarrow a_1^{\downarrow} t_2^{\uparrow\uparrow}$	1.41 (1.06)	1.42	1.77
0	$a_1^2 t_2^{\uparrow\uparrow} \rightarrow a_1^{\downarrow} t_2^{\uparrow\uparrow\uparrow}$	1.42 (1.07)	1.44	1.82
−	$a_1^2 t_2^{\uparrow\uparrow\uparrow} \rightarrow a_1^{\rightarrow} t_2^{\uparrow\uparrow\uparrow} t_2^{\downarrow}$	1.60 (1.40)	1.57	1.40
2−	$a_1^2 t_2^{\uparrow\uparrow\uparrow} t_2^{\downarrow} \rightarrow a_1^{\uparrow} t_2^{\uparrow\uparrow\uparrow} t_2^{\downarrow\downarrow}$	1.43 (1.23)	1.73	1.68

sites possess larger (smaller) energies for positively charged or neutral (negatively charged) Si vacancies than those at cubic sites.

The values in table 2 approach the experimental findings [19–21]. Son *et al* [19] relate the PL line at 1.12 eV for 3C to a $S = 1/2$ centre, probably V_{Si}^{+}. We follow this interpretation, in particular because of the spin state. From the point of view of the energy, one cannot exclude V_{Si}^{0}. However, neither the spin $S = 1$ nor the spin $S = 0$ fits the PL experiments, in contrast to the corresponding vacancy in diamond [50]. The conclusions from the comparison are more vague in the case of 4H, despite the reduced dispersion of the lowest defect band as a consequence of the hexagonal crystal field. The transition energies 1.44 and 1.82 eV calculated without dispersion corrections for V_{Si}^{0} approach the positions of the two zero-phonon PL lines at 1.35 and 1.44 eV accompanied by an $S = 1$ signal measured with optically detected magnetic resonance (ODMR) [20, 21]. However, such an interpretation is doubtful because of the spin state and the larger computed line splitting. Another possible explanation of the occurrence of two lines for 4H may be related to the crystal-field splitting of the $t_2^{\uparrow}$ level into $a_1^{\uparrow}$ and $e^{\uparrow}$ ones and not to the two inequivalent sites. Taking into account a dispersion correction of 0.31 eV, the transition in V_{Si}^{2-} can also be considered for the interpretation. Spin state and line splitting agree with the measurements.

5. Complexes with boron

There is usually no direct access to the atomic and electronic structures of defects, in particular not to those of defect complexes. On the other hand more direct studies, especially of the geometry, are possible near surfaces. In order to contribute to a clarification of the problem of doping with boron, we therefore study the adsorption of B atoms on SiC surfaces. The vacuum region may be considered to simulate the presence of vacancies near to the B atoms. Since the bilayer stacking is less important for the surface structure [34], the Si-terminated SiC(111)$\sqrt{3} \times \sqrt{3}$R30° adatom surface of 3C-SiC is investigated as a model surface. Eleven adsorption geometries and stoichiometries are investigated. We find the two surface geometries in figure 6 to be stable. Both conserve the Si adatom in a T_4 position.

Under more C-rich preparation conditions, B substitutes for a Si basis atom of the Si adatom (figure 6(a)). This is in agreement with bulk experiments. A coimplantation of C and B atoms leads to a competition for the occupation of a site in the C sublattice, so boron occupies a Si site [27]. Similar results are observed for layers grown by CVD with low Si/C ratio [51] or by solid-source MBE [52]. Since the B adatom appears in the first atomic layer below the vacuum region, the resulting configuration may be related to a boron–vacancy complex in the bulk, e.g. B_{Si}–V_C. Under Si-rich conditions the B adatom replaces a C atom in the subsurface region (see figure 6(b)). The result may be interpreted as a substitutional impurity, B_C.

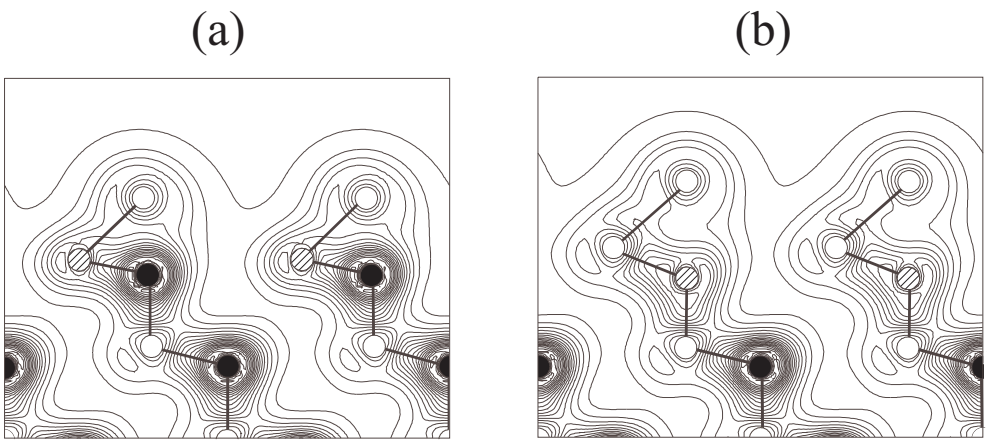

Figure 6. Electron density near a SiC(111)$\sqrt{3} \times \sqrt{3}$ surface projected onto a (110) plane. Shaded (open, full) circle: B (Si, C) atom. Results for the two most favourable configurations (a) and (b) are plotted.

The two B-induced geometries give rise to completely different electronic structures as indicated by the surface band structures in figure 7. In the case (a) of substituting a Si atom, no filled surface states appear in the fundamental gap of 3C-SiC. There is only a pronounced empty mid-gap band that is related to Si dangling bonds and combinations of B–C antibonding orbitals which could also occur in a B_{Si}–V_C complex. Electrons are transferred from the Si dangling bonds (of the C vacancy in the bulk) into B–C bonds. In the case (b), replacing a carbon atom in the second atomic layer, boron induces surface bands that are energetically not very different from bulk SiC states. Filled B-related bands occur slightly below the valence band maximum. Besides those of B–Si bonding orbitals there are also strong contributions from the Si dangling bonds to the underlying wave functions. We suggest experimental studies

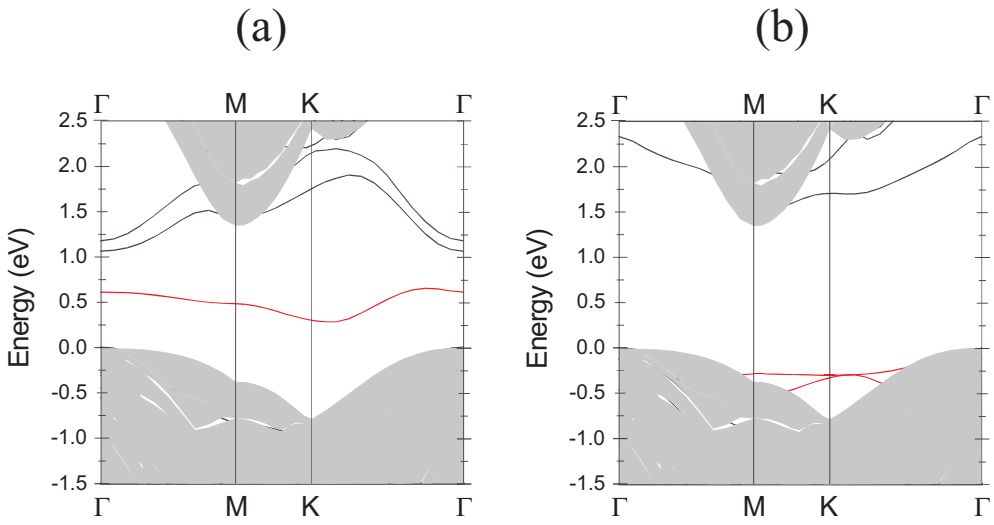

Figure 7. Band structures of the two most stable B adsorbates (a) and (b) on SiC(111)$\sqrt{3} \times \sqrt{3}$. The projected bulk band structure is indicated by shaded regions.

of the geometrical and electronic structure of the boron adsorbates in order to clarify the nature of bulk B-related acceptors.

6. Summary

In the case of wide-band-gap semiconductors such as SiC, *first-principles* calculations also allow the description of geometrical, thermodynamic, and electronic properties of defects or defect complexes. In the paper this is mainly demonstrated for native defects. Monovacancies have been considered as prototypical defects. However, to a certain extent antisites and vacancy complexes have also been discussed. We have shown that in thermodynamic equilibrium the carbon vacancy should have the lowest formation energies in bulk SiC independent of the polytype. It forms a double donor which dramatically reduces the doping efficiency of acceptors as Al atoms. The theory also allows the calculation of energies of optical transitions between bulk and vacancy states or excited and ground states of vacancies. We discussed their possible relationship to recent photoluminescence measurements. The preparation-dependent behaviour of boron with respect to occupation of Si or C lattice sites and the possible formation of complexes with vacancies is demonstrated by studying the B adsorption on a SiC surface.

Acknowledgments

The authors acknowledge financial support from the Deutsche Forschungsgemeinschaft (Sonderforschungsbereich 196, projects A3 and A8). Some of the computations were done at the J von Neumann Institute for Computing in Jülich.

References

[1] Jepps N W and Page T F 1983 *Prog. Cryst. Growth Charact.* **7** 259
[2] Choyke W J, Hamilton D R and Patrick L 1964 *Phys. Rev.* **133** A1163
[3] Bechstedt F and Käckell P 1995 *Phys. Rev. Lett.* **75** 2180
[4] Itoh H, Hayakawa N, Nashiyama I and Sakuma E 1989 *J. Appl. Phys.* **66** 4529
[5] Zywietz A, Furthmüller J and Bechstedt F 1999 *Phys. Rev.* B **59** 15 166
[6] Torpo L, Pöykkö S and Nieminen R 1998 *Phys. Rev.* B **57** 6243
[7] Wang C, Bernholc J and Davis R F 1988 *Phys. Rev. B* **38** 12 752
[8] Schneider J and Maier K 1993 *Physica* B **185** 199
[9] Choyke W J 1990 *The Physics and Chemistry of Carbides, Nitrides and Borides (NATO Advanced Study Institute Series E, vol 185: Applied Sciences)* ed R Freer (Dordrecht: Kluwer Academic) p 563
[10] Makarov V V 1972 *Sov. Phys.–Solid State* **13** 1974
[11] Haberstroh Ch, Helbig R and Stein R A 1994 *J. Appl. Phys.* **76** 509
[12] Egilsson T, Bergmann J P, Ivanov I G, Henry A and Janzen E 1999 *Phys. Rev.* B **59** 1956
[13] Egilsson T, Henry A, Ivanov I G, Lindström J L and Janzen E 1999 *Phys. Rev.* B **59** 8008
[14] Kennedy T A, Freitas J A and Bishop S G 1990 *J. Appl. Phys.* **68** 6170
[15] Nishino K, Kimoto T and Matsunami H 1995 *Japan. J. Appl. Phys.* **34** L1110
[16] Fissel A, Richter W, Furthmüller J and Bechstedt F 2001 *Appl. Phys. Lett.* **78** 2512
[17] Choyke W J, Fenc Z C and Powell J A 1988 *J. Appl. Phys.* **64** 3163
[18] Zywietz A, Furthmüller J and Bechstedt F 2000 *Phys. Rev.* B **61** 13 655
[19] Son N T, Sörman E, Chen W M, Singh M, Hallin C, Kordina O, Monemar B and Janzen E 1996 *J. Appl. Phys.* **79** 3784
[20] Sörman E, Son N T, Chen W M, Kordina O, Hallin C and Janzen E 2000 *Phys. Rev.* B **61** 2613
[21] Wagner M, Magnusson B, Chen W M, Janzen E, Sörman E, Hallin C and Lindström J L 2000 *Phys. Rev.* B **62** 16 555
[22] Van Duijn-Arnold A, Ikoma T, Poluektov O G, Baranov P G, Mokhov E N and Schmidt J 1998 *Phys. Rev.* B **57** 1607
[23] Gali A, Deak P, Devaty R P and Choyke W J 1999 *Phys. Rev.* B **60** 10 620

[24] Fukumoto A 1996 *Phys. Rev.* B **53** 4458
[25] Van Duijn-Arnold A, Mol J, Verberk R, Schmidt J, Mokhov E N and Baranov P G 1999 *Phys. Rev.* B **60** 15 829
[26] Bockstedte M, Mattausch A and Pankratov O 2001 *Mater. Sci. Forum* **353–356** 447
[27] Frank T, Troffer T, Pensl G, Nordell N, Karlsson S and Schöner A 1998 *Mater. Sci. Forum* **264–268** 681
[28] Hohenberg P and Kohn W 1964 *Phys. Rev.* **136** B864
[29] Kohn W and Sham L J 1965 *Phys. Rev.* **140** A1133
[30] Kresse G and Furthmüller J 1996 *Comput. Mater. Sci.* **6** 15
Kresse G and Furthmüller J 1996 *Phys. Rev.* B **54** 11 169
[31] Furthmüller J, Käckell P, Bechstedt F and Kresse G 2000 *Phys. Rev.* B **61** 4576
[32] Perdew J P and Zunger A 1981 *Phys. Rev.* B **23** 5048
[33] von Barth U and Hedin L 1972 *J. Phys. C: Solid State Phys.* **5** 1629
[34] Bechstedt F, Zywietz A, Karch K, Adolph B, Tenelsen K and Furthmüller J 1997 *Phys. Status Solidi* b **202** 35
[35] Wenzien B, Käckell P, Bechstedt F and Cappellini G 1995 *Phys. Rev.* B **52** 10 897
[36] Monkhorst H J and Pack J D 1976 *Phys. Rev.* B **13** 5188
[37] Grossner U, Furthmüller J and Bechstedt F 2001 *Phys. Rev.* B submitted
[38] Baraff G A, Kane E O and Schlüter M 1980 *Phys. Rev.* B **21** 5662
[39] Bechstedt F, Zywietz A and Furthmüller J 1998 *Europhys. Lett.* **44** 309
[40] Torpo L, Nieminen R M, Laasonen K E and Pöykkö S 1999 *Appl. Phys. Lett.* **74** 221
[41] Zywietz A, Furthmüller J and Bechstedt F 1998 *Phys. Status Solidi* b **210** 13
[42] Deak P, Miro J, Gali A, Udvardi L and Overhof H 1999 *Appl. Phys. Lett.* **75** 2103
[43] Zywietz A, Furthmüller J and Bechstedt F 2000 *Phys. Rev.* B **62** 6854
[44] Zhang S B and Northrup J E 1991 *Phys. Rev. Lett.* **67** 2339
[45] Itoh H, Kawasuro A, Ohshima T, Yoshikawa M, Nashiyama I, Tanigawa S, Misawa S, Okumura H and Yoshida S 1997 *Phys. Status Solidi* a **162** 173
[46] Kim H J and Davis R F 1986 *J. Electrochem. Soc.* **133** 2350
[47] Yamanaka M, Daimon H, Sakuma E, Misawa S and Yoshida S 1987 *J. Appl. Phys.* **61** 599
[48] Langer J M and Heinrich H 1985 *Phys. Rev. Lett.* **55** 1414
[49] Rauls E, Lingner T, Hajnal Z, Greulich-Weber S, Fraunheim T and Spaeth J-M 2000 *Phys. Status Solidi* b **217** R1
[50] Davies G, Lawson S C, Collins A T, Mainwood A and Sharp S J 1992 *Phys. Rev.* B **46** 13 157
[51] Sridhara S G, Clemen L L, Devaty R P, Choyke W J, Larkin D J, Kong H S, Troffer T and Pensl G 1998 *J. Appl. Phys.* **83** 7909
[52] Fissel A 2001 *J. Cryst. Growth* **805** 227